Draft version July 15, 2025

Typeset using LaTeX **twocolumn** style in AASTeX631

CHIME/FRB Discovery of an Unusual Circularly Polarized Long-Period Radio Transient with an Accelerating Spin Period

Fengqiu Adam Dong,[1,2] Kaitlyn Shin,[3,4] Casey Law,[5,6] Mason Ng,[7,8,9] Ingrid Stairs,[10] Geoffrey Bower,[11,12] Alyssa Cassity,[10] Emmanuel Fonseca,[13,14] B. M. Gaensler,[15,16,17] Jason W. T. Hessels,[7,8,18,19] Victoria M. Kaspi,[7,8] Bikash Kharel,[13,14] Calvin Leung,[20,21] Robert A. Main,[7,8] Kiyoshi W. Masui,[3,4] James W. McKee,[22] Bradley W. Meyers,[23,24] Obinna Modilim,[3] Ayush Pandhi,[17,16] Aaron B. Pearlman,[7,8,25,26,9] Scott M. Ransom,[1] Paul Scholz,[27,16] and Kendrick Smith[28]

[1] *National Radio Astronomy Observatory, 520 Edgemont Rd, Charlottesville, VA 22903, USA*

[2] *Green Bank Observatory, 155 Observatory Road, WV 24944, USA*

[3] *MIT Kavli Institute for Astrophysics and Space Research, Massachusetts Institute of Technology, 77 Massachusetts Ave, Cambridge, MA 02139, USA*

[4] *Department of Physics, Massachusetts Institute of Technology, 77 Massachusetts Ave, Cambridge, MA 02139, USA*

[5] *Cahill Center for Astronomy and Astrophysics, MC 249-17 California Institute of Technology, Pasadena CA 91125, USA*

[6] *Owens Valley Radio Observatory, California Institute of Technology, Big Pine CA 93513, USA*

[7] *Department of Physics, McGill University, 3600 rue University, Montréal, QC H3A 2T8, Canada*

[8] *Trottier Space Institute, McGill University, 3550 rue University, Montréal, QC H3A 2A7, Canada*

[9] *FRQNT Postdoctoral Fellow*

[10] *Department of Physics and Astronomy, University of British Columbia, 6224 Agricultural Road, Vancouver, BC V6T 1Z1 Canada*

[11] *Academia Sinica Institute of Astronomy and Astrophysics, 645 N. A'ohoku Pl., Hilo, HI 96720, USA*

[12] *East Asian Observatory, 660 N. A'ohoku Pl., Hilo, HI 96720, USA*

[13] *Department of Physics and Astronomy, West Virginia University, PO Box 6315, Morgantown, WV 26506, USA*

[14] *Center for Gravitational Waves and Cosmology, West Virginia University, Chestnut Ridge Research Building, Morgantown, WV 26505, USA*

[15] *Department of Astronomy and Astrophysics, University of California, Santa Cruz, 1156 High Street, Santa Cruz, CA 95060, USA*

[16] *Dunlap Institute for Astronomy and Astrophysics, 50 St. George Street, University of Toronto, ON M5S 3H4, Canada*

[17] *David A. Dunlap Department of Astronomy and Astrophysics, 50 St. George Street, University of Toronto, ON M5S 3H4, Canada*

[18] *Anton Pannekoek Institute for Astronomy, University of Amsterdam, Science Park 904, 1098 XH Amsterdam, The Netherlands*

[19] *ASTRON, Netherlands Institute for Radio Astronomy, Oude Hoogeveensedijk 4, 7991 PD Dwingeloo, The Netherlands*

[20] *Miller Institute for Basic Research, University of California, Berkeley, CA 94720, United States*

[21] *Department of Astronomy, University of California, Berkeley, CA 94720, United States*

[22] *Department of Physics and Astronomy, Union College, Schenectady, NY 12308, USA*

[23] *International Centre for Radio Astronomy Research (ICRAR), Curtin University, Bentley WA 6102, Australia*

[24] *Australian SKA Regional Centre (AusSRC), Curtin University, Bentley WA 6102, Australia*

[25] *Banting Fellow*

[26] *McGill Space Institute Fellow*

[27] *Department of Physics and Astronomy, York University, 4700 Keele Street, Toronto, ON MJ3 1P3, Canada*

[28] *Perimeter Institute of Theoretical Physics, 31 Caroline Street North, Waterloo, ON N2L 2Y5, Canada*

ABSTRACT

We report the discovery of CHIME J1634+44, a Long Period Radio Transient (LPT) unique for two aspects: it is the first known LPT to emit fully circularly polarized radio bursts, and it is the first LPT with a significant spin-up. Given that high circular polarization ($> 90\%$) has been observed in FRB 20201124A and in some giant pulses of PSR B1937+21, we discuss the implications of the high circular polarization of CHIME J1634+44 and conclude its emission mechanism is likely to be "pulsar-like". While CHIME J1634+44 has a pulse period of 841 s, its burst arrival patterns are indicative of a secondary 4206 s period, probably associated with binary activity. The timing properties suggest it has a significantly negative period derivative of $\dot{P} = -9.03(0.11) \times 10^{-12}$ s s^{-1}. Few systems have been known to spin-up, most notably transitional millisecond pulsars and cataclysmic binaries, both of which seem unlikely progenitors for CHIME J1634+44. If the period was only associated with the spin of the object, then the spin up is likely generated by accretion of material from a companion. If,

however, the radio pulse period and the orbital period are locked, as appears to be the case for two other LPTs, the spin up of CHIME J1634+44 could be driven by gravitational wave radiation.

1. INTRODUCTION

In recent years, a new class of "Long Period Radio Transients" (LPTs) have been discovered, with periods ranging from tens of seconds to hours (Hurley-Walker et al. 2022; Caleb et al. 2022; Hurley-Walker et al. 2023; Caleb et al. 2024; Dong et al. 2024; de Ruiter et al. 2025; Hurley-Walker et al. 2024; Wang et al. 2024; Li et al. 2024; Lee et al. 2025). LPTs have been named as such due to their long radio periods compared to pulsars, while still producing coherent emission. The emission of LPTs is required to be coherent as these sources are bright and detected at low frequencies (less than 300 MHz in some cases; Hurley-Walker et al. 2022, 2023), implying a non-physical brightness temperature (Manchester & Taylor 1977; Hurley-Walker et al. 2022).

Two models have arisen as likely progenitors for LPTs — magnetic white dwarfs (WDs), and neutron stars (NSs) (Katz 2022; Beniamini et al. 2023; Rea et al. 2024). These models are favored due to two classes of known astrophysical objects that produce coherent radio emission, WD pulsars and NS pulsars. In the LPT population, we find evidence for both source types. For example, two LPTs, ILT J1101+5521 and GLEAM-X J0704–37, are WDs in a binary orbit with M dwarf stars, confirmed via optical spectroscopy (de Ruiter et al. 2025; Hurley-Walker et al. 2024; Rodriguez 2025). WD binary LPTs pulse on periods of hours, much longer than the rotation period of WD pulsars(minutes; Marsh et al. 2016; Buckley et al. 2017; Pelisoli et al. 2023). In fact, WD binary LPTs pulse on periods similar to that of the orbit of WD binary pulsar systems. Other LPTs, like PSR J0901-4046, are most likely isolated NSs. This is demonstrated through a stable pulse profile, indicating persistent beamed emission like a NS pulsar (Caleb et al. 2022). It is becoming increasingly clear that there may be two different populations of LPTs, namely those that exist in WD binaries and those that are slowly rotating neutron stars.

Here, we report the discovery of a new LPT discovered by the Canadian Hydrogen Intensity Mapping Experiment (CHIME)/Fast Radio Burst (FRB)/Pulsar survey for Galactic pulsars, CHIME J1634+44. This source was independently co-discovered during the LOFAR Two-meter Sky Survey Data Release 2 (Shimwell et al. 2019, 2022) as part of a Stokes V transient search (Bloot et al., 2025). In Section 2, we detail the telescopes and modes of operation that were used. Section 3 details the measurements made by the VLA. Section 4 details a search for optical counterparts. Section 5 provides a long baseline timing solution and poses several conundra in CHIME J1634+44's timing properties. Finally, we discuss the results and possible implications of the CHIME J1634+44 system in Section 6.

2. DISCOVERY AND OBSERVATIONS

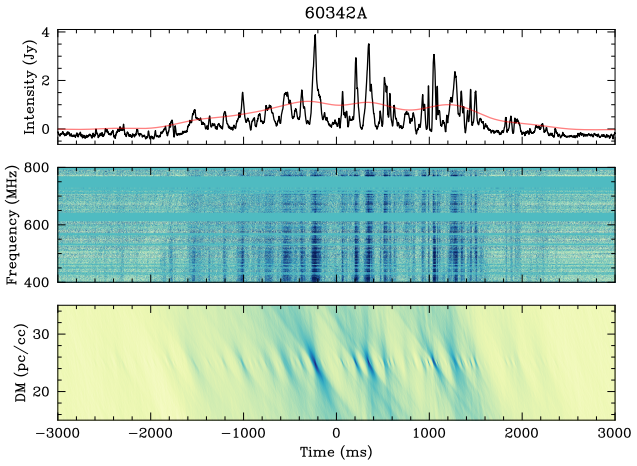

Figure 1. Sample of a detection made with the CHIME/Pulsar instrument. The top panel shows the dedispersed flux-calibrated frequency-averaged profile. The red line is the smoothed profile for TOA extraction, the middle panel shows the dedispersed dynamic spectrum, and the bottom panel shows the DM-time power spectrum. The title is the MJD the burst was detected, following the convention in Dong et al. (2024).

CHIME is a transit radio telescope in British Columbia, Canada. It consists of four 20x100 m cylindrical dishes. The unique cylindrical design allows for a wide instantaneous field of view of ∼200 square degrees over the 400-800 MHz bandwidth in observing frequency. While CHIME's primary goal is to detect hydrogen at cosmological distances (CHIME Collaboration et al. 2022), the large spatial and frequency coverage enables CHIME to perform rapid all-sky daily surveys for pulsars, FRBs, and other transient events. CHIME, therefore, conducts multiple commensal experiments like CHIME/FRB (CHIME/FRB Collaboration et al. 2018) and CHIME/Pulsar (CHIME/Pulsar Collaboration et al. 2021).

CHIME J1634+44 was discovered in the CHIME/FRB single pulse pulsar survey, where we are using the CHIME/FRB trigger criteria (CHIME/FRB Collaboration et al. 2018) for all sources with a disper-

sion measure (DM) low enough to be considered inside the Milky Way Galaxy according to both the NE2001 and the YMW16 DM models (Cordes & Lazio 2002; Yao et al. 2017). This survey utilizes the full observing capabilities of the 1024 Fast Fourier Transformed beams to survey the CHIME sky (CHIME/FRB Collaboration et al. 2018). We discovered the first burst from CHIME J1634+44 on MJD 59883 (2022 October 31). We observed multiple instances of reactivation after that, beginning on MJD 60003 (2023 February 28) and then again for a longer activation timespan on MJD 60270 (2023 November 22). During this timespan, we identified a period of ∼841 s. A search through archival metadata of CHIME/FRB revealed that there were bursts from CHIME J1634+44 dating back to MJD 58893 (2022 February 14). These bursts only have trigger information, such as timestamps, signal-to-noise (S/N), and DM. We can confirm that they are indeed astrophysical as they phase connect with CHIME J1634+44 bursts that have been verified. Activity epochs of CHIME J1634+44 were sporadic, but we retrieved channelized raw voltage data (hereafter referred to as baseband data, CHIME/FRB Collaboration et al. 2024a) after MJD 60270 (2023 November 22).

CHIME/Pulsar tracking beam observations record 327.68 μs dynamic spectra in SIGPROC filterbank format [1]. The first detection made with CHIME/Pulsar was on MJD 60270 (2023 December 23). An example is shown in Figure 1[2].

The sudden active state of CHIME J1634+44 on MJD 60270 (2023 November 22) resulted in Director's Discretionary Time (DDT) observations with the Karl G. Jansky Very Large Array (VLA), utilizing the *realfast* system at 10 ms integrations and visibility data at 2 s integrations for 4 hours (23B-337). We also triggered Target of Opportunity (ToO) observations using the *Neil Gehrels Swift X-ray Telescope (Swift)* for 10 ks (target ID 16412) and the Green Bank Telescope (GBT) for 4 hours at 680-920 MHz. Both the GBT and the VLA detected two bursts. The VLA/*realfast* detections led to a localization of (RA, Dec) = (16h34m29.96s±0.5″, +44d50m13.5s±1.1″)[3]. The *Swift XRT* data showed no sources within the 3-σ localization error region; however, we place an upper limit on the 0.3–10 keV luminosity $L_X < 1.3 - 5.2 \times 10^{32}$ ergs s^{-1} depending on the model used. Details are provided in Appendix C.

[1] https://sigproc.sourceforge.net/

[2] The rest of the detection plots, including those by CHIME/FRB, are provided at https://github.com/CHIMEFRB/J1634-44_additional_information

[3] All coordinates are given in the J2000 reference frame.

To summarize all of the detections, the most extensive set was made with the CHIME/FRB and CHIME/Pulsar instruments, which detected 69 and 44 bursts, respectively. The two instruments frequently detected the same bursts. The GBT and the VLA detected 2 bursts each. In total, 89 unique bursts were detected over a ∼ 4.5 yr period.

We calculate the quasiperiod on all bursts that show significant microstructure via an autocorrelation function and a Fast Fourier Transform (FFT). the details are presented in Appendix A.6. Quasiperiodicity indeed exists among many bursts emitted by CHIME J1634+44 with a median quasiperiod of $P_\mu = 0.13(11)$ s. We find that this does not align well with the universal NS quasiperiod relation described by Kramer et al. (2024).

We flux calibrated all bursts from CHIME/Pulsar using three calibrators which bracket the CHIME J1634+44 declination range. They are 3C380, 3C196, and NGC1265 at declinations of +48.75°, +48.22°, and +41.9°, respectively. The procedure is described in Appendix A.1 and Dong (2024). The dispersion measure is calculated via variance optimization of the DM-time power spectrum and further describe in Appendix A.2.

3. VERY LARGE ARRAY

The *realfast* search system triggered on two unique bursts from CHIME J1634+44 at MJD 60301.76197 and 60301.85935 topocentric time. The detection was made at the edge of the triggered buffer window for both bursts, so we can only provide a lower limit on the temporal width of the bursts of roughly 3 seconds. Due to the temporal width and higher observing frequency, the DM is poorly constrained compared to the CHIME measurements.

We calibrated and imaged the 9 s fast visibility data in the band with the strongest burst emission (128 MHz centered at 1392 MHz) to measure the burst polarization and the source position. The triggered recording only includes the two auto-correlation products, RR and LL. As shown in Figure 2, the RR and LL polarization images show that CHIME J1634+44 differs from all other sources in the image in that it is only detected in the RR correlation product. We find the source to be spatially unresolved with a mean flux of 77±1 mJy in the RR correlation product. In the LL product, we measure an upper limit of 1.8 mJy (3 sigma). This implies a lower limit on the circular polarization fraction of 98%. We provide the specific technical details of the VLA observations in Appendix A.5

3.1. *Astrometry*

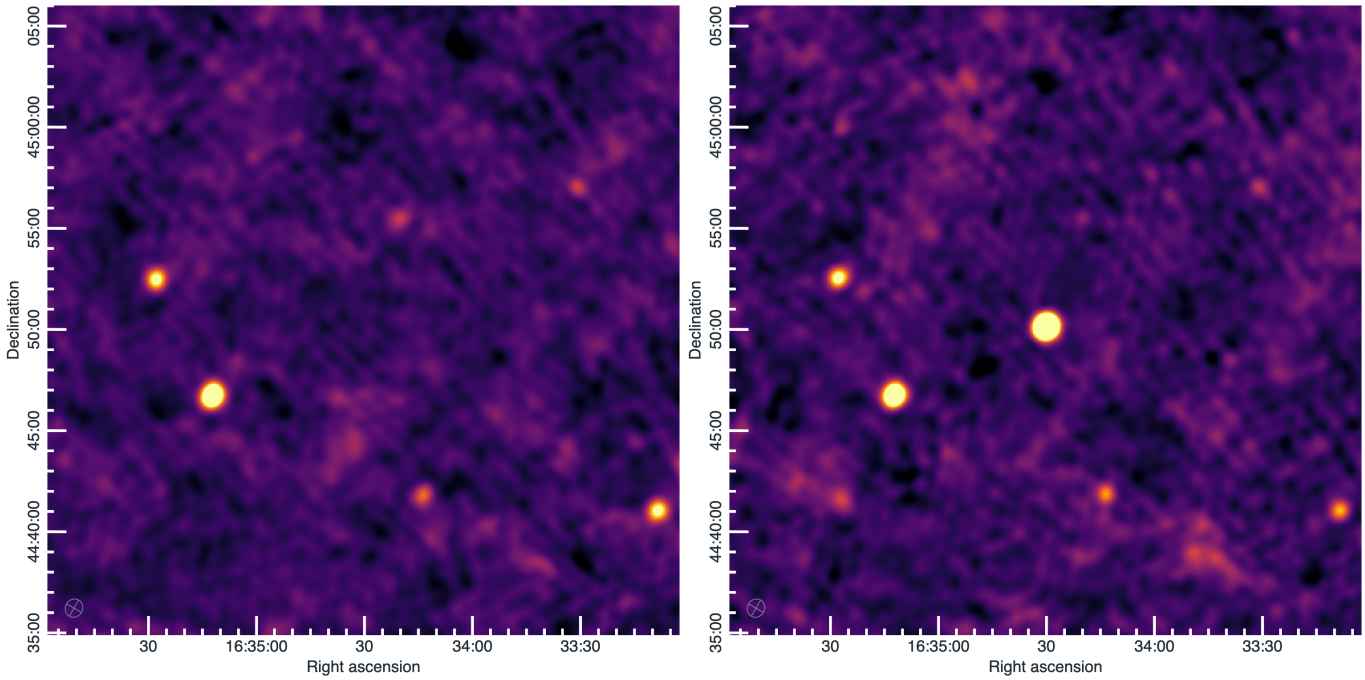

Figure 2. VLA radio continuum images of the LL and RR correlation products toward CHIME J1634+44. The images were made from visibilities selected from the entire 9 s triggered data time span and frequencies from 1328 to 1456 MHz. The source is only significantly detected in RR polarization, which is consistent with 100% circular polarization.

We find a best-fit source position with a statistical error of 0.3″ using the RR image. However, the absolute astrometry of the VLA is typically limited by gain calibration to roughly 1/20th of the synthesized beam size of 46″(White et al. 1997). To improve on this, we directly measure the astrometric accuracy for this image by matching radio sources in the field to sources cataloged in the FIRST survey (version 2014Dec17; Helfand et al. 2015). Since FIRST has an astrometric error of 20 milliarcsec, we expect the astrometry of CHIME J1634+44 to be limited by the statistical errors in the primary measurement.

Four of the seven nearest radio sources seen in Figure 2 have unresolved counterparts in FIRST. To make the CHIME J1634+44 astrometry consistent with FIRST, we must apply a mean shift of (ΔRA, ΔDec) = $(-0.7, 2.7)''$. After applying this shift, we find the position of CHIME J1634+44 to be (RA, Dec) = (16h34m29.96s +44d50m13.5). Treating the scatter of the cross-matched sources as an estimate of the astrometric precision, we find a total position 1σ uncertainty of $(0.5'', 1.1'')$. These errors should be treated as an upper limit on the astrometric precision caused by cross-matched calibration sources; the lower limit is the statistical error in the primary measurement of 0.3″.

4. OPTICAL

Due to the presence of optical counterparts to some discovered LPTs (de Ruiter et al. 2025; Hurley-Walker et al. 2024), we searched through archival data to determine the presence of possible optical counterparts to CHIME J1634+44. Public data on this field of view are available from the Hyper Suprime-Cam (HSC) via the HSC Subaru Strategic Program third public data release (HSC-SSP PDR3; Aihara et al. 2022) and the HSC Legacy Archive (HSCLA; Tanaka et al. 2021). These are the deepest publicly available observations of this field. Within the 3-σ, but outside the 2-σ localization region determined by VLA/*realfast* (Section 3.1), one optical source is visible (Figure 3) in HSC data.

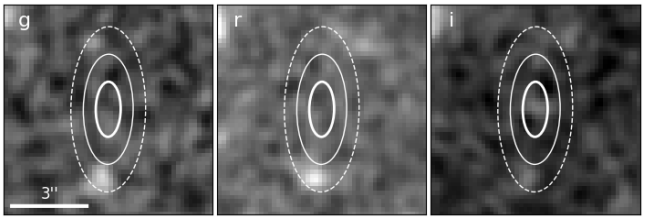

Figure 3. Archival optical imaging from HSC, smoothed and centered on the VLA/*realfast* localization for CHIME J1634+44; up is North and left is East. The g-band image from the PDR3, and the r- and i-band images are from the HSCLA. Overlaid on the images are 1-σ, 2-σ, and 3-σ contours in bold, solid, and dashed lines. The possible optical source is at the bottom of the 3-σ contours, most visible in the g- and r-band images.

While HSC observes in *grizy* filters, in the public data release, photometry was only successfully determined for this source in the g and r filters. Visual inspection of the PDR3 coadded images confirms that this source is not significantly detected in redder filters. In the HSCLA observations of this field, there appears to be a marginal source in the i filter; however, it is too faint to extract reliable photometry. The Kron magnitudes of this source are $m_{\mathrm{AB},g} = 25.3 \pm 0.4$ and $m_{\mathrm{AB},r} = 25.5 \pm 0.8$. The 5-$\sigma$ limiting magnitudes around this source for the other filters are $m_{\mathrm{AB},i} = 25.4$, $m_{\mathrm{AB},z} = 24.4$, and $m_{\mathrm{AB},y} = 23.4$.

We estimate a chance alignment probability by obtaining all the HSC PDR3 sources within a 3° radius around the VLA/*realfast* localization of CHIME J1634+44, that also have g-band and r-band photometry at least as bright as this optical candidate source. We draw 10^6 random positions within this region and determine the number of times a drawn position lies within 3.3″(the 3-σ uncertainty in Dec) of an optical source; we find this occurs ≈5.8% of the time.

Given its classification by the HSC pipeline as extended rather than point-like, and the separation from the VLA localization, it is possible that this optical source is a background object (e.g., a background galaxy) rather than a true optical counterpart. Even if we assume that the classification as an extended source is incorrect (plausible because of its faint magnitude), the possible interpretation of this optical source is relatively limited given our two faint photometric data points. The optical source appears to be tentatively brighter in the g- band than the r- band, which may be promising for a WD progenitor given the rise of the spectral energy distribution towards bluer wavelengths; however, we did not find u-band data for this source, and there is no detection in the UV in archival *GALEX* (Martin et al. 2005) data. If this optical source were a true counterpart to CHIME J1634+44, consistent WD temperatures could range from ∼20,000 K to ∼40,000 K. The optical source being brighter in g- band than in r- band is inconsistent with the expected spectral energy distribution of an M dwarf. However, at the DM-inferred distance of CHIME J1634+44, the presence of a faint late-M dwarf cannot be ruled out.

5. TIMING

This section provides the methodology for the timing analysis of CHIME J1634+44. All the provided TOAs are topocentric at the position of the respective observatories. We use PINT (Luo et al. 2021) for the barycentering, frequency correction, and the timing model fit of the data. The TOA errors on each burst are large enough such that the clock offsets between the CHIME/FRB instrument and the CHIME/Pulsar instruments are insignificant in comparison (Dong et al. 2024). Nevertheless, we found all coincident detections between CHIME/Pulsar and CHIME/FRB and fit the frequency, the first frequency derivative, and a global timing offset between the two datasets. The resultant offset is 0.3(3) s. For the rest of the timing analysis, we proceed with this value fixed as the timing offset between these two data sets. We provide the full timing solution in Table 1.

CHIME J1634+44 was initially identified to possess a period of ∼ 4206 s (70.1 minutes). With this period and CHIME's short ∼ 10 minute transit, we expect to make a detection of CHIME J1634+44 every second day. This 2-day spacing is a beat period between 4206 s and CHIME's observation cadence. This spin period appeared robust until MJD 60348, when we detected two bursts on consecutive days. This detection confirmed the need for a shorter period of ∼841 s. However, this posed other concerns. If the period was indeed 841 s, why did most of our bursts occur with a 2-day spacing? We find that the number of bursts we detect with a 2-day separation (i.e., in agreement with 4206 s) has a probability of occurring by random chance of 3.5×10^{-9} (shown in Appendix B). This is discussed further in Section 6.

Table 1.

R.A. (hh:mm:ss)*	16h34m29.96s
Dec (dd:mm:ss)*	44°50'13.5"
P(s)	841.245895(6)
$\dot{P}(\times 10^{-12}$ ss$^{-1})$	–9.03(0.11)
PEPOCH(MJD)	60366
TIMEEPH	FB90
NTOA	127
CLOCK	TT(BIPM2023)
RMS Residuals (phase)	0.0055
RMS Residuals (s)	4.6
Derived Values	
Galactic Longitude (deg)	70.17
Galactic Latitude (deg)	+42.58

* These are fixed at the VLA positions.

With an 841 s period, the residuals show some scatter relative to the typical TOA error. The residual scatter is about 2% of the period, roughly similar to the duty cycles found in Hurley-Walker et al. (2024) and de Ruiter et al. (2025). However, the bursts from CHIME J1634+44 appear to be narrower than the aforementioned sources. The overall timing residuals are still small compared to the period ($\lesssim |1|\%$). It also appears

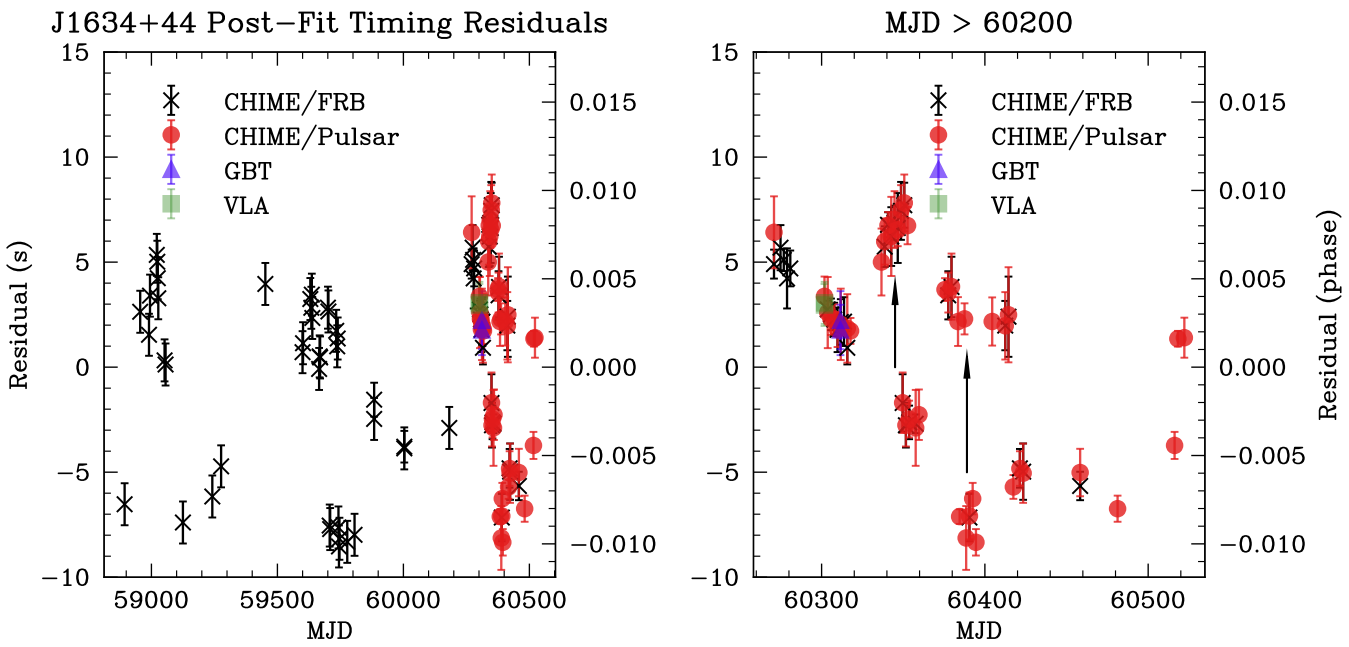

Figure 4. Residuals for a 841 s period. The error bars are 1σ. The right panel shows a zoomed-in image of the densest portion of TOAs when all instruments were observing CHIME J1634+44. The arrows show offsets possibly due to timing noise between burst as discussed in the text.

that there are some scatter between bursting epochs in the data. For example, see the right panel arrows in Figure 4. This may be caused by timing noise. The period derivative for CHIME J1634+44 is negative at > 80-σ, indicating that there are additional physics that the timing process does not capture, e.g., possible accretion of material onto CHIME J1634+44, as radiating objects are generally expected to lose rotational energy and spin down (increasing period). We discuss the possible implications of the negative period derivative in Section 6.

6. DISCUSSION

6.1. *Polarization*

The polarization of CHIME J1634+44 is rare among the radio emissions emitted by compact objects. It is challenging to produce 100% circular polarization at the luminosities observed. Fully circularly polarized radio pulses or bursts have been observed in main sequence stars such as the Sun (Dulk 1985), CU Vir (e.g., Lo et al. 2012), M dwarfs (e.g, YZ Ceti, YZ CMi; Pineda & Villadsen 2023; Rucinski 1994), auroral (or magnetospheric) processes around cool brown dwarfs (Hallinan et al. 2007, 2008), magnetic cataclysmic variables (e.g. Barrett et al. 2020), and the Jovian system (e.g., Marques et al. 2017). These are all close by (within 75 pc) and produce pulses three orders of magnitude lower in flux than CHIME J1634+44, resulting in five orders of magnitude lower luminosities. It is thus unlikely that CHIME J1634+44 shares the same underlying emission mechanisms as any of these objects.

There is strong evidence that some Fast Radio Bursts (FRBs) are produced by NSs through magnetar bursts (CHIME/FRB Collaboration et al. 2020; Bochenek et al. 2020) or pulsar emission (Mckinven et al. 2024; Nimmo et al. 2025). Recently, FRB 20201124A has been observed to produce ∼90% circularly polarized bursts (Jiang et al. 2024). Most pulsars have low circular polarization (Han et al. 1998). However, PSR B1937+21 has shown that the brightest giant pulses can be almost fully circularly polarized (Cognard et al. 1996). Giant pulses are usually offset from the main radio components, as shown in the case of PSR B1937+21 (Cognard et al. 1996) and PSR B0540-69 (Johnston et al. 2004). They are, however, aligned with the X-ray and/or γ–ray emission, suggesting a common origin (Enoto et al. 2021). Scaling PSR B1937+21 to the distance of CHIME J1634+44, our X-ray detection threshold of 1.2×10^{-13}erg cm^{-2} s^{-1} should have detected something PSR B1937+21-like (Cusumano et al. 2003), but as discussed in Section 6.2, X-ray pulsars can be much fainter than PSR B1937+21. This is suggestive that CHIME J1634+44 may produce as-of-yet undetected high-energy pulsations. While the emission mechanisms for giant pulses remain highly debated, the mechanisms that generate "normal" coherent radiation from pulsars are likely curvature radiation and/or in-

verse Compton scattering of particle bunches (Lorimer & Kramer 2012). Both models require a line of sight off-center from the radiation axis to create the fully circularly polarized bursts we observe. Emission from particle bunches, particularly, can produce highly circularly polarized bursts despite being only slightly off-axis (Jiang et al. 2024).

Regardless of the source, propagation effects could also cause circular polarization. For example, generalized Faraday rotation (also called Faraday conversion) can partially convert linearly polarized light to circularly polarized (Vedantham & Ravi 2019; Qu & Zhang 2023). However, this does not usually result in fully circularly polarized bursts as we have observed in CHIME J1634+44. Additionally, these effects are frequency-dependent; the LOFAR-CHIME-VLA measurements (Bloot et al., 2025) show that fully circularly polarized bursts remain robust over a decade in observing frequencies. Therefore, we conclude that the circular polarization is intrinsic to CHIME J1634+44.

We conclude that "pulsar-like" emission mechanisms are the most likely for CHIME J1634+44 as fully circularly polarized bursts have been observed from NSs at the energetics required.

6.2. *X-ray counterparts*

Multiwavelength detections of CHIME J1634+44 can enable further characterization of its origin. For example, the X-ray detection of DART/ASKAP J1832−0911 may suggest it is an older ($\gtrsim 0.5\,\mathrm{Myr}$) magnetar or a highly-magnetized WD in a WD-M dwarf binary (see Wang et al. (2024)). Although the age may be debated due to the supernovae remnant coincident found by Li et al. (2024).

Our observations with Swift/XRT were also triggered while CHIME J1634+44 was active, Assuming a DM-inferred distance of 1.4–3 kpc, we calculate an upper limit on the 0.3–10 keV luminosity of $5.2 \times 10^{31}\,\mathrm{ergs\,s^{-1}}$ or $1.3 \times 10^{32}\,\mathrm{ergs\,s^{-1}}$ assuming a blackbody spectrum ($kT = 0.3\,\mathrm{keV}$, representative of a magnetar; Hurley-Walker et al. 2022) or a power law spectrum ($\Gamma = 1$, representative of a polar; Rodriguez et al. 2023) specified above, respectively. This is about a factor of 6 lower than DART/ASKAP J1832−0911, suggesting different origins.

Magnetars often have radiative outbursts accompanying radio emission of X-ray bolometric luminosities of $L_X \gtrsim 10^{34}\,\mathrm{ergs\,s^{-1}}$ (Coti Zelati et al. 2018), two orders of magnitude higher than our limit. However, CHIME J1634+44 could be a quiescent magnetar, though it would be among the least luminous quiescent magnetars known (Coti Zelati et al. 2018; Hu et al. 2019). Alternatively, CHIME J1634+44 could be a high magnetic field rotationally powered NS. For example, PSR 1937−3333 has an $L_X \approx 2 \times 10^{32}\,\mathrm{ergs\,s^{-1}}$ (Olausen et al. 2013), which is at the edge of our detection limit.

If CHIME J1634+44 contains a magnetic WD, it could be an intermediate polar system where the spins are synchronized with the orbital period. While typical intermediate polars have luminosities $L_X > 10^{33}\,\mathrm{ergs\,s^{-1}}$ (Salcedo et al. 2024), CHIME J1634+44 could belong to the class of low-luminosity intermediate polars where $L_X \approx 10^{30-31}\,\mathrm{ergs\,s^{-1}}$, for which only a handful are known (Salcedo et al. 2024).

We conclude from *Swift XRT* observations that we can rule out the brightest X-ray emitters such as active magnetars. Still, we cannot rule out high magnetic field NSs or low-luminosity intermediate polars. Though the latter are likely rarer

6.3. *Negative Period Derivative*

Through timing, we find that the period derivative is nonphysical (negative at $> 80\sigma$) for an isolated source. This suggests additional intriguing physical mechanisms of the system, such as accreting matter from a companion, which we will discuss in this section. We note that CHIME J1634+44 is the first LPT to exhibit a significant negative $\dot{P}$. GLEAM-X J0704−37 (Hurley-Walker et al. 2024) have also shown hints of negative period derivatives, albeit at low significance, and likely caused by noise fluctuations of the time of arrivals. A similar scenario for the spin-up of CHIME J1634+44 could be that infalling material from a binary companion is providing CHIME J1634+44 with angular momentum. Transitional millisecond pulsars (Wijnands & van der Klis 1998; Papitto & de Martino 2022) and cataclysmic variables (Warner 1995; Schreiber et al. 2021) have been observed to have spin ups ranging from $\dot{\nu} \approx 4 - 8 \times 10^{-13}\mathrm{Hz/s}$ (see section 6.3.2 of Papitto & de Martino 2022) and $\dot{\nu} \approx 10^{-7} - 10^{-12}\mathrm{Hz/s}$ (see Table 1 of Schaefer 2024), respectively. These measurements have furthered the understanding of millisecond pulsars and the evolution of binary white dwarves. Therefore, if the radio period of CHIME J1634+44 was only associated with the central engine, then accretion is a likely scenario.

Rodriguez (2025) found that the orbital period of GLEAM-X J0704−37 was equal to the radio pulse period of 2.9 hours (Rodriguez 2025). ILT J1101+5521 is also a similar system (de Ruiter et al. 2025). If we speculate that CHIME J1634+44 is also in a compact binary where the radio pulse period and the orbital pe-

riod are locked at 841 s (14.02 minutes), then a natural explanation for the significant $\dot{P}$ is orbital decay via gravitational wave emission. Indeed, such systems have already been observed in short-period WD-WD binaries (Burdge et al. 2019a,b), with orbital periods of 6.91 and 20.6 minutes.

We calculate the chirp mass, M_c, given our timing constraints by solving for M_c in the equation

$$2\dot{f} = \frac{96}{5}\pi^{(8/3)}(2f)^{(11/3)}\frac{(GM_c)^{(5/3)}}{c^5} \quad (1)$$

where $\dot{f}$ is the orbital spin-up rate, f is the orbital frequency, G is the gravitational constant, and c is the speed of light. We find that the chirp mass is $M_c = 0.36$ solar masses and defined by

$$M_c = \frac{(m_1 m_2)^{3/5}}{(m_1 + m_2)^{1/5}}. \quad (2)$$

By integrating Equation 1, we also calculate that the merger time scale is ∼1,100,000 years, and assuming a circular orbit, Kepler's third law gives us that the semi-major axis is 0.00065 AU (15 Earth Radii, 0.14 Sun Radii).

This constrains the component stars to WD-NS or WD-WD systems. In the WD-WD scenario, both stars must be at the upper range of WD masses. Known cases of main sequence stars binaries which are compact enough, such as AM Canum Venaticorum, have component stars which are only ∼ 0.1 solar masses (Solheim 2010), too low mass to work in this scenario. We further note that AM Canum Venaticorum systems are predicted to produce detectable gravitational waves by future space-based observatories (Solheim 2010). Given what we speculate here, CHIME J1634+44 could be an additional candidate for such observatories.

This analysis assumes that the orbit is shrinking purely due to angular momentum loss via gravitational wave (GW) radiation. However, other factors may also affect the orbit, such as tidal deformation and magnetic field interactions between the component stars (Burdge et al. 2019a).

6.4. *4206 s bursting pattern*

We showed in Section 5 and Appendix B that given a 841 s period, we see an over abundance of pulses which agree with a 4206 s period. The pulsing pattern of CHIME J1634+44 is unique. Usually, one pulse is produced every five rotations of the 841 s period (i.e., one pulse every 4206 s period), but occasionally, two pulses can be produced every five rotations. When this happens, it is nearly always offset by 2 rotations of the 841 s (or 0.4 in phase of the 4206 s period). Pulsars and LPTs are known to produce interpulses (Manchester & Lyne 1977; Lee et al. 2025); therefore, we may be detecting a main pulse and an interpulse. For the interpulse scenario to be accurate, we must assume four interpulse components, all separated by almost exactly a phase of 0.2. Heretofore, no pulsar or WD system has been observed to exhibit such an interpulse structure. Therefore, we believe that the interpulse scenario is unlikely.

An alternative hypothesis is that CHIME J1634+44 is in a binary system with spin-orbit resonances. Indeed, due to this effect, Bloot et al. (2025) propose a 2103 s binary orbit in a 5:2 resonance. Although we find no evidence for the specific configuration proposed by Bloot et al. (2025), the discussion presented above argues that a binary model may be necessary to explain the observations.

6.5. *Is CHIME J1634+44 an NS or WD?*

Neutron Star Model:—As previously discussed, NSs have been observed to emit pulsed coherent radio emission as luminous or even more so in the form of FRBs and giant pulses, while being fully circularly polarized. While our X-ray non-detection in the active state of CHIME J1634+44 can rule out active magnetars, they do not preclude rotationally-powered X-ray emitting NSs. The microstructure of CHIME J1634+44 is strongly reminiscent of other confirmed pulsars like XTE 1810−197 (Maan et al. 2019) and PSR J0901−4046 (Caleb et al. 2022). No such microstructure with significant quasiperiod has been identified in pulsating WDs before. Finally, CHIME J1634+44 is likely in a binary system. Neutron star systems have shown they can exist in binaries and exhibit spin-up. For example, in the case of transitional millisecond pulsars (Jaodand et al. 2018; Falanga et al. 2005).

White Dwarf Model—There is an optical counterpart at the edge of the 3-σ localization of CHIME J1634+44 which could indicate a 20000-40000 K WD. However, we estimate a chance alignment probability of ≈6%. Deeper observations are required.

The WD binary luminosities pose a problem for CHIME J1634+44. From the dispersion measure, CHIME J1634+44 resides at a distance of 1.4–3 kpc, with a peak flux of ∼0.4-9 Jy. The two WD pulsars, AR Scorpii (Marsh et al. 2016; Buckley et al. 2017) and J191213.72–441045.1 (Pelisoli et al. 2023), were found at a distance of 117 pc and 237 pc, respectively with flux densities of ∼ 4-10 mJy. While the total fluence of their pulses is not provided, if we assume similar effective widths, the energies emitted by CHIME J1634+44

are 5-6 orders of magnitude greater than those emitted by AR Scorpii and J191213.72–441045.1. Therefore, we conclude that the magnetic interaction mechanisms proposed for the WD pulsars will struggle to explain the emissions by CHIME J1634+44. Compared to WD-MD binaries, ILT J1101+5521 and GLEAM-X J0704-37, CHIME J1634+44 emits radio bursts 2-3 orders of magnitude greater in energy. Therefore, we conclude that similar emission mechanisms are unlikely.

Finally, like pulsars, WD binaries can be in cataclysmic variables which exhibit spin-up, for example, in intermediate polar systems (e.g. Paice et al. 2024).

Given these arguments, particularly those regarding the luminosity and polarization of CHIME J1634+44, we conclude CHIME J1634+44 is more likely to be a NS-like system than a WD-like system.

To conclude, we have discovered a fully circularly polarized long period radio transient (LPT) source, CHIME J1634+44. It has been localized with the Karl Jansky Very Large Array to $\sim 1''$ precision. CHIME J1634+44 possesses a period of 841 s (∼14 minutes) but clearly shows a secondary period at 4206 s, possibly associated with binary activity. Furthermore, CHIME J1634+44 has a significantly negative period derivative, implying intriguing physics, such as gravitational wave radiation, which could be occurring. From arguments due to luminosity and polarization, we believe that CHIME J1634+44 is NS-like. CHIME J1634+44 will serve as an important test bed for LPT emission theories and is unique among the array of known transient source emitters.

7. ACKNOWLEDGMENTS

We thank Ryan Lynch for his support in calibrating the GBT data.

F.A.D. is supported by a Jansky Fellowship. K.S. is supported by the NSF Graduate Research Fellowship Program. C.J.L. has been supported by NSF award 2022546. M.N. is a Fonds de Recherche du Québec – Nature et Technologies (FRQNT) postdoctoral fellow. Pulsar and FRB research at UBC is supported by an NSERC Discovery Grant and by the Canadian Institute for Advanced Research. E.F. is supported by the National Science Foundation under grant AST-2407399. J.W.T.H. and the AstroFlash research group acknowledge support from a Canada Excellence Research Chair in Transient Astrophysics (CERC-2022-00009). V.M.K. holds the Lorne Trottier Chair in Astrophysics & Cosmology, a Distinguished James McGill Professorship, and receives support from an NSERC Discovery grant (RGPIN 228738-13). C. L. is supported by the Miller Institute for Basic Research at UC Berkeley. K.W.M. holds the Adam J. Burgasser Chair in Astrophysics. A.P. is funded by the NSERC Canada Graduate Scholarships – Doctoral program. A.B.P. is a Banting Fellow, a McGill Space Institute (MSI) Fellow, and a Fonds de Recherche du Quebec – Nature et Technologies (FRQNT) postdoctoral fellow. The National Radio Astronomy Observatory is a facility of the National Science Foundation operated under cooperative agreement by Associated Universities, Inc. SMR is a CIFAR Fellow and is supported by the NSF Physics Frontiers Center award 2020265. P.S. acknowledges the support of an NSERC Discovery Grant (RGPIN-2024-06266).

We acknowledge that CHIME is located on the traditional, ancestral, and unceded territory of the Syilx/Okanagan people. We are grateful to the staff of the Dominion Radio Astrophysical Observatory, which is operated by the National Research Council of Canada. CHIME is funded by a grant from the Canada Foundation for Innovation (CFI) 2012 Leading Edge Fund (Project 31170) and by contributions from the provinces of British Columbia, Québec and Ontario. The CHIME/FRB Project, which enabled development in common with the CHIME/Pulsar instrument, is funded by a grant from the CFI 2015 Innovation Fund (Project 33213) and by contributions from the provinces of British Columbia and Québec, and by the Dunlap Institute for Astronomy and Astrophysics at the University of Toronto. Additional support was provided by the Canadian Institute for Advanced Research (CIFAR), McGill University and the McGill Space Institute thanks to the Trottier Family Foundation, and the University of British Columbia. The CHIME/Pulsar instrument hardware was funded by NSERC RTI-1 grant EQPEQ 458893-2014.

This research was enabled in part by support provided by the BC Digital Research Infrastructure Group and the Digital Research Alliance of Canada (alliancecan.ca).

The National Radio Astronomy Observatory and Green Bank Observatory are facilities of the U.S. National Science Foundation operated under cooperative agreement by Associated Universities, Inc.

This work made use of data supplied by the UK Swift Science Data Centre at the University of Leicester and the Swift satellite. Swift, launched in November 2004, is a NASA mission in partnership with the Italian Space Agency and the UK Space Agency. Swift is managed by NASA Goddard. Penn State University controls science and flight operations from the Mission Operations Center in University Park, Pennsylvania. Los Alamos

National Laboratory provides gamma-ray imaging analysis.

8. SOFTWARE AND THIRD PARTY DATA REPOSITORY CITATIONS

Facilities: CHIME, GBT, VLA, Swift(XRT and UVOT), HSC

Software: Numpy, Astropy, sigpyproc3, Presto

APPENDIX

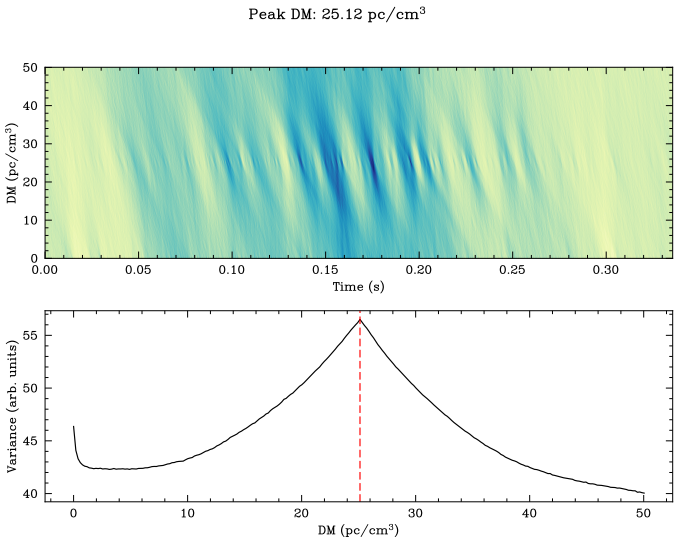

Figure 5. Example of a DM-time power spectrum from burst 60311A, detected by CHIME/Pulsar between 400-800 MHz. The bottom panel shows the variance across the DM of the top panel.

A. DETECTIONS

We provide tables for all the detections from CHIME/FRB, CHIME/Pulsar, the GBT, and the VLA in Tables 2, 3, and 4. Where possible, we provide the fluence, effective width, peak flux density, and pseudo-luminosity. The MJD is referenced at 800 MHz for CHIME/Pulsar, 400 MHz for CHIME/FRB, 920 MHz for the GBT and 1440 MHz for the VLA.

A.1. *Flux Density and Fluence*

Flux density is difficult to estimate for CHIME/FRB due to a complex beam response (Andersen et al. 2023). Furthermore, as the CHIME/FRB total intensity data segment can be slightly shorter than the pulse width, it is difficult to get a steady off-source measurement. For this reason, we provide CHIME/FRB data only in arbitrary units. In general, flux calibration with the CHIME/Pulsar instrument is simpler due to the tracking of phased array beams and longer observation tracks. With the CHIME/Pulsar instrument, daily calibration observations are taken. We use three calibrators that bracket the CHIME J1634+44 declination range. These calibrators are 3C380, 3C196, and NGC1265 at declinations of +48.75°, +48.22°, and +41.9°, respectively. The calibrators are used to determine the telescope temperature, $T_{\rm telescope}$, which includes the receiver, structure, and ground temperatures. The calibration is done by solving the following equation:

$$S_{\rm src} = \frac{(T_{\rm sky} + T_{\rm telescope}) \times ({\rm ON} - {\rm OFF})}{G \times {\rm OFF}}, \tag{A1}$$

where $S_{\rm src}$ is the flux density of the calibrator in Jy, ON and OFF are the raw counts of the on and off source integrations respectively, and G is the gain of the phased array beam in K/Jy. $T_{\rm sky}$ is the sky temperature in K, which is determined by the Haslam 408 MHz all-sky continuum map (Haslam et al. 1982). $T_{telescope}$ is calibrated by fitting a polynomial to the catalog values of the calibrators. A full discussion of the CHIME/Pulsar flux density calibration pipeline is given by Dong (2024). The fluence is the time-integrated value across the whole burst, and the effective width is the fluence divided by the peak flux density.

A.2. *Dispersion Measure*

The DM is determined by calculating the variance over time in the dispersion-time power spectrum for each trial dedispersion (lowest panel in Figure 1). The variance is used instead of the summed intensity because as the hot-spot structure spreads, the total power is distributed over time but not significantly diminished. We then find the peak that is not at 0, which is taken to be the optimal DM of the burst. We show an example in Figure 5. The mean of

Table 2. Detection results for CHIME/Pulsar observations

Observation	MJD (Topocentric)	Fluence (Jyms)	Effective width (ms)	Peak flux density (Jy)	Pseudo-luminosity* ($Jykpc^2$)
CHIME/Pulsar	60270.84871(2)	140(30)	80(30)	1.7(3)	3.3
CHIME/Pulsar	60301.76199(1)	900(200)	300(100)	3.2(6)	6.3
CHIME/Pulsar	60303.75793(2)	2000(400)	500(200)	3.9(8)	7.6
CHIME/Pulsar	60305.753885(9)	1000(200)	300(100)	3.4(7)	6.7
CHIME/Pulsar	60307.749838(8)	2100(400)	700(300)	2.8(6)	5.5
CHIME/Pulsar	60309.74578(1)	1100(200)	500(200)	2.3(5)	4.5
CHIME/Pulsar	60311.74173(2)	1400(300)	700(300)	2.1(4)	4.1
CHIME/Pulsar	60315.73362(2)	5000(1000)	700(300)	8(2)	15.7
CHIME/Pulsar	60317.729565(7)	2000(400)	400(200)	4.7(9)	9.2
CHIME/Pulsar	60336.66665(2)	4400(900)	400(100)	12(2)	23.5
CHIME/Pulsar	60338.66260(1)	700(100)	230(90)	3.2(6)	6.3
CHIME/Pulsar	60340.658534(7)	500(100)	220(90)	2.3(5)	4.5
CHIME/Pulsar	60342.65446(2)	2000(400)	500(200)	3.9(8)	7.6
CHIME/Pulsar	60344.65040(2)	1700(300)	600(300)	2.6(5)	5.1
CHIME/Pulsar	60346.646318(9)	2000(400)	700(300)	2.9(6)	5.7
CHIME/Pulsar	60348.64226(1)	1500(300)	300(100)	4.4(9)	8.6
CHIME/Pulsar	60349.63525(2)	1400(300)	700(300)	1.8(4)	3.5
CHIME/Pulsar	60350.63819(2)	1600(300)	400(200)	3.9(8)	7.6
CHIME/Pulsar	60351.63116(1)	270(50)	150(60)	1.8(4)	3.5
CHIME/Pulsar	60352.63411(1)	4000(800)	800(300)	5(1)	9.8
CHIME/Pulsar	60353.62709(1)	800(200)	190(80)	4.0(8)	7.8
CHIME/Pulsar	60357.61895(2)	700(100)	300(100)	2.6(5)	5.1
CHIME/Pulsar	60359.61488(1)	1000(200)	170(70)	6(1)	11.8
CHIME/Pulsar	60375.562934(6)	60(10)	70(30)	0.9(2)	1.8
CHIME/Pulsar	60377.55887(1)	2400(500)	500(200)	4.5(9)	8.8
CHIME/Pulsar	60379.55481(2)	1200(200)	500(200)	2.5(5)	4.9
CHIME/Pulsar	60383.54667(1)	2100(400)	400(100)	6(1)	11.8
CHIME/Pulsar	60384.539665(4)	80(20)	160(60)	0.5(1)	1.0
CHIME/Pulsar	60387.538556(9)	460(90)	220(90)	2.1(4)	4.1
CHIME/Pulsar	60388.53154(2)	70(10)	180(70)	0.42(8)	0.8
CHIME/Pulsar	60390.52750(1)	500(100)	140(50)	3.5(7)	6.9
CHIME/Pulsar	60392.523456(9)	1800(400)	500(200)	3.8(8)	7.4
CHIME/Pulsar	60394.519381(7)	1700(300)	300(100)	6(1)	11.8
CHIME/Pulsar	60404.47981(1)	2400(500)	300(100)	9(2)	17.6
CHIME/Pulsar	60412.46367(2)	1700(300)	700(300)	2.7(5)	5.3
CHIME/Pulsar	60414.45965(3)	900(200)	700(300)	1.3(3)	2.5
CHIME/Pulsar	60417.448649(7)	800(200)	300(100)	2.7(5)	5.3
CHIME/Pulsar	60421.44062(1)	1300(300)	400(200)	3.4(7)	6.7
CHIME/Pulsar	60423.43660(2)	1500(300)	500(200)	2.8(6)	5.5
CHIME/Pulsar	60458.34241(1)	150(30)	180(70)	0.8(2)	1.6
CHIME/Pulsar	60481.272590(7)	100(20)	120(50)	0.8(2)	1.6
CHIME/Pulsar	60516.179617(7)	900(200)	300(100)	2.7(5)	5.3
CHIME/Pulsar	60518.175765(4)	50(10)	110(40)	0.47(9)	0.9
CHIME/Pulsar	60522.15821(1)	500(100)	150(60)	3.5(7)	6.9

* This is given as a lower limit by using the lower estimate of the distance, 1.4 kpc.

Table 3. Detection results for CHIME/FRB observations

Observation	MJD (Topocentric)	Observation	MJD (Topocentric)
CHIME/FRB metadata	58893.62626(1)	CHIME/FRB intensity	59883.914336(9)
CHIME/FRB metadata	58955.45209(1)	CHIME/FRB intensity	60003.584379(9)
CHIME/FRB metadata	58990.35777(1)	CHIME/FRB intensity	60270.848702(8)
CHIME/FRB metadata	58994.34984(1)	CHIME/FRB intensity	60274.84070(1)
CHIME/FRB metadata	59021.27218(1)	CHIME/FRB intensity	60276.836688(6)
CHIME/FRB metadata	59023.26824(1)	CHIME/FRB intensity	60278.83267(2)
CHIME/FRB metadata	59025.26430(1)	CHIME/FRB intensity	60280.82866(1)
CHIME/FRB metadata	59027.26036(1)	CHIME/FRB intensity	60303.757945(5)
CHIME/FRB metadata	59052.18699(1)	CHIME/FRB intensity	60305.753897(9)
CHIME/FRB metadata	59056.17917(1)	CHIME/FRB intensity	60307.749847(9)
CHIME/FRB metadata	59124.99057(1)	CHIME/FRB intensity	60309.74579(1)
CHIME/FRB metadata	59241.67340(1)	CHIME/FRB intensity	60311.74174(1)
CHIME/FRB metadata	59276.57788(1)	CHIME/FRB intensity	60313.73769(1)
CHIME/FRB metadata	59452.09220(1)	CHIME/FRB intensity	60315.733622(9)
CHIME/FRB metadata	59599.69042(1)	CHIME/FRB intensity	60338.66260(1)
CHIME/FRB metadata	59601.68636(1)	CHIME/FRB intensity	60340.658543(7)
CHIME/FRB metadata	59630.60303(1)	CHIME/FRB intensity	60342.65447(2)
CHIME/FRB metadata	59634.59489(1)	CHIME/FRB intensity	60344.65040(1)
CHIME/FRB metadata	59636.59083(1)	CHIME/FRB intensity	60346.64633(2)
CHIME/FRB metadata	59638.58675(1)	CHIME/FRB intensity	60348.64227(2)
CHIME/FRB metadata	59665.50760(1)	CHIME/FRB intensity	60349.63526(2)
CHIME/FRB metadata	59667.50357(1)	CHIME/FRB intensity	60350.63820(1)
CHIME/FRB metadata	59669.49952(1)	CHIME/FRB intensity	60351.63117(1)
CHIME/FRB metadata	59700.41284(1)	CHIME/FRB intensity	60353.627102(9)
CHIME/FRB metadata	59702.40883(1)	CHIME/FRB intensity	60357.618958(5)
CHIME/FRB metadata	59707.39385(1)	CHIME/FRB intensity	60377.55888(1)
CHIME/FRB metadata	59709.38986(1)	CHIME/FRB intensity	60379.55482(2)
CHIME/FRB metadata	59733.32280(1)	CHIME/FRB intensity	60390.52751(1)
CHIME/FRB metadata	59737.31488(1)	CHIME/FRB intensity	60412.46368(1)
CHIME/FRB metadata	59739.31093(1)	CHIME/FRB intensity	60414.45966(2)
CHIME/FRB metadata	59742.30003(1)	CHIME/FRB intensity	60421.44063(1)
CHIME/FRB metadata	59744.29607(1)	CHIME/FRB intensity	60423.43661(2)
CHIME/FRB metadata	59746.29213(1)	CHIME/FRB intensity	60458.342412(8)
CHIME/FRB metadata	59777.20691(1)		
CHIME/FRB metadata	59806.12589(1)		
CHIME/FRB metadata	60182.09721(1)		

Table 4. Detection results for VLA and GBT observations

Observation	MJD (Topocentric)	Fluence (Jyms)	Effective width (ms)	Peak flux density (Jy)	Pseudo-luminosity* (Jykpc^2)
VLA	60301.76197(1)	–	–	–	–
VLA	60301.85935(1)	–	–	–	–
GBT	60311.54701(1)	3100(300)	900(90)	3.5(4)	6.9
GBT	60311.59569(2)	2900(300)	1100(100)	2.7(3)	5.3

* This is given as a lower limit by using the lower estimate of the distance, 1.4 kpc.

the DM for all bursts is calculated to be 25.0(2) pc cm^{-3}, where the uncertainty is the standard error on the mean. Throughout this work, we assume that this is the true DM of CHIME J1634+44. We note that there appears to be no significant DM evolution of CHIME J1634+44.

The inferred DM distance for this direction is 1.4 kpc and 3.0 kpc for the NE2001 (Cordes & Lazio 2002) and YMW16 (Yao et al. 2017) dispersion models, respectively.

A.3. *Time of Arrival Determination*

Arrival times for pulses are required for determining a phase-coherent timing model CHIME J1634+44. Because of significant microstructure in the pulses, we extract this information by applying a 200 ms Gaussian filter across each burst so that the microstructure is fully smoothed over. This technique has similarly been used by Hurley-Walker et al. (2022) and Dong et al. (2024). The TOA and 1 σ errors are defined as the peak and the full-width-half-maximum of the smoothed profile, respectively. For the metadata-only detections, we report these bursts with a TOA error of 1 s and assume that the burst has been dedispersed to the optimal DM by the CHIME/FRB Bonsai pipeline (CHIME/FRB Collaboration et al. 2018).

A.4. *CHIME Polarization Measurements*

From August 2023 through April 2024, 24 observed bursts from CHIME J1634+44 triggered the raw voltage data recording system for CHIME/FRB (Michilli et al. 2021; CHIME/FRB Collaboration et al. 2024b). While the overarching burst envelopes have durations of ∼seconds (Figure 1), due to data buffer constraints, only ∼100 ms of raw voltage data are saved per burst. These voltage data are saved with a 2.56 μs time and ∼390 kHz frequency resolution, and full Stokes information. We can thus conduct polarimetry analysis on these bursts despite the limited temporal extent of the written data.

We use the CHIME/FRB polarimetry pipeline developed for FRBs, as detailed by Mckinven et al. (2021) and Pandhi et al. (2024), with a few modifications to the defaults described by those works. Off-burst data are necessary for determining noise statistics when obtaining polarization fractions. While the standard voltage data products for FRBs encompass both on-burst and off-burst extents, for CHIME J1634+44, there is no true off-burst data within the data span. To remedy this, for the seven events where sub-burst structure in the raw voltage data were S/N $>$ 10, we take their respective written data and beamform the files to both the best position provided by VLA/*realfast* for our on-burst data and 0.5 degrees lower in declination for our off-burst data. We form our off-position beam lower in declination, as the CHIME primary beam model varies much more rapidly in RA than in Dec (CHIME Collaboration et al. 2022). All bursts were de-dispersed to DM = 25.0 pc cm^{-3}.

The Faraday rotation measure (RM) is determined by both non-parametric methods (rotation measure synthesis; Burn 1966; Brentjens & de Bruyn 2005) and parametric methods (QU-fitting; adapted from the `RM-tools` package, Purcell et al. 2020). Both measurements suffer from instrumental systematics, particularly a non-trivial leakage effect between Stokes U and V values introduced by a non-zero physical delay between the two linear polarizations (cable delay). This cable delay can also introduce a sign ambiguity to the measured RM signal. Rather than adopt the default model used by Mckinven et al. (2021) and Pandhi et al. (2024) where the assumption is that there is no significant circular polarization intrinsic to the burst (i.e., $|V|/I \lesssim 0.2$), we adopt a model where the QU-fitting routine allows for a non-zero circularly polarized component with a power-law spectrum.

CHIME J1634+44 appears to have a low RM, with detections of signal ranging from RM ~ -12 rad m^{-2} to $\sim +11$ rad m^{-2}, with no clear sign preference between the RM synthesis and QU-fitting results. We check the Galactic RM map by Hutschenreuter et al. (2022) and find RM$_{\rm gal} = 19 \pm 5$ rad m^{-2}; this measurement is a cumulative sum of RM along the entire Galactic line of sight. A nearby pulsar ∼5° away, J1638+4005, also has RM = 17 rad m^{-2}. We thus conclude that CHIME J1634+44 has an RM in line with expectations from the intervening interstellar medium, and that there is no evidence for a dense, magnetized circumburst environment. Furthermore, our measurements are consistent with Bloot et al. 2025.

Consistent with the VLA/*realfast* data, all these CHIME bursts showed evidence for significant intrinsic circular polarization, with $|V|/I \gtrsim 0.9$. All bursts also showed evidence for non-negligible intrinsic linear polarization, with $|L|/I \gtrsim 0.2$. Exact fractions and uncertainties are not reported, as despite the attempts to correct for instrumental effects, there are likely still instrumental sources of circular polarization of $\gtrsim$20% (Pandhi et al. 2024).

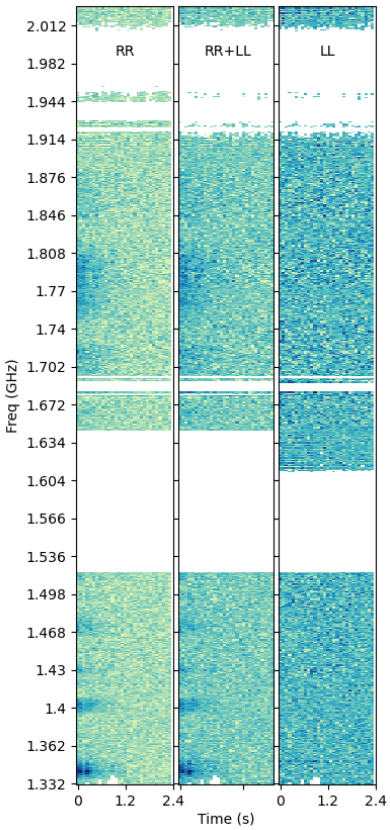

Figure 6. Dynamic spectrum for a portion of the first burst of CHIME J1634+44 seen by VLA/*realfast*. The realfast search system detected this burst at the boundary of a buffer, so this plot only shows the second half of the first burst. The three panels show the RR, RR+LL (Stokes I), and LL polarization products. The time and frequency span of all three panels is identical.

A.5. *Karl G. Jansky Very Large Array*

To better localize the radio bursts and search for multiwavelength counterparts, we observed CHIME J1634+44 with the Karl G. Jansky Very Large Array (VLA) under program code 23B-337. The observations used the *realfast* commensal fast transient search system to detect the bursts, which outputs 10 ms visibilities, much shorter than the shortest 2 s integrations of standard VLA observations (Law et al. 2018).

A single 4-hour observation was executed on 23 December 2023. The VLA was in its most compact ("D") configuration with 26 antennas available. We observed the position of CHIME J1634+44 in the 1–2 GHz ("L") band, which is the lowest supported by *realfast*, and which minimized the extrapolation from the expected flux from CHIME. The synthesized beam size had a full-width at half-maximum of 46″.

The observation was designed to provide basic gain calibration for the transient search. The flux calibrator was 3C286 and the gain calibrator was J1625+4134. Target scans were 2 minutes long and the on-target observing efficiency was roughly 85%.

Each scan produced standard correlated visibility output with 2-second time resolution and a fast copy with 10-ms time resolution. The fast copy was sent to the *realfast* transient search pipeline. The standard visibility data included all four cross-correlation products, but *realfast* receives only the self-correlation products, RR and LL. Both data streams included a frequency span from 1–2 GHz, covered by 16 subbands of 64 channels each (channel width of 1 MHz).

The *realfast* system forms Stokes I images over a range of DMs and timescales (Law et al. 2018). The mean visibility is subtracted during the transient search, so any image with a significant source will likely be a transient signal (either

astrophysical or interference). A simple threshold is used to trigger the recording of fast visibility data for offline analysis.

In total, this observation produced 17 candidates above a detection threshold of 7.2. The threshold was defined to allow 0.1 false events per scan, or roughly nine false events total. From these 17 candidates, two bursts were identified as astrophysical with signal-to-noise ratios of 8.9 and 8.4 in images made on the longest real-time search width of 80 ms. The rest of the detections were RFI.

Figure 6 shows the dynamic spectrum for the first burst. The triggered fast visibility data span 9 seconds, but only the 2.4 seconds near the burst are shown in the figure. The burst is seen across most of the observing band, but is strongest below 1450 MHz.

A.6. *Quasiperiodicity*

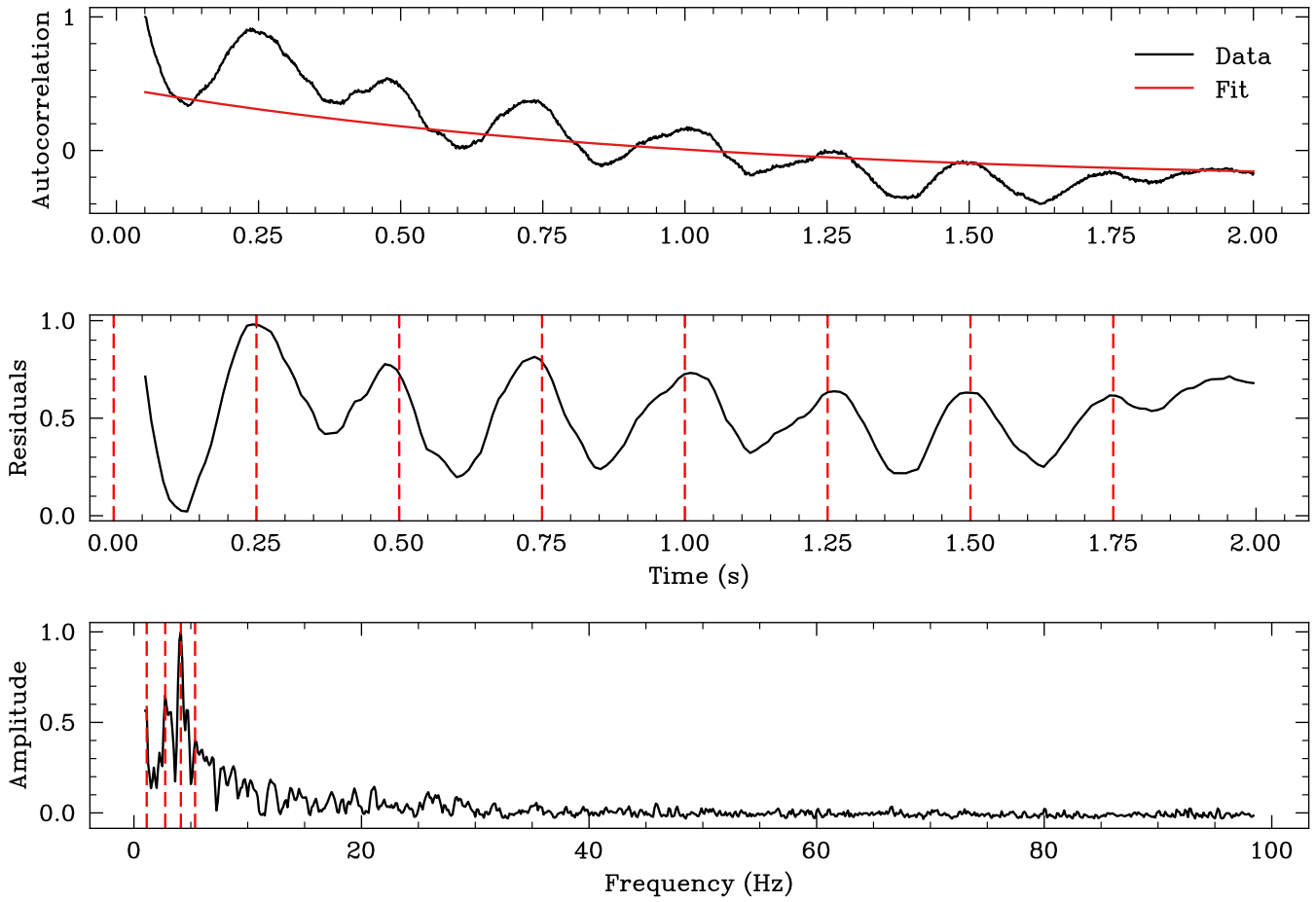

Figure 7. An example of the autocorrelation function and the FFT power spectrum from burst 60309A. The top panel shows the raw autocorrelation function normalized to 1. The middle panel shows a subtraction of the exponentially decaying baseline, an approximation to the red noise. The quasiperiod is identified at ∼4 Hz and marked in the red dotted lines. The bottom panel shows the FFT power spectrum. The red dashed lines show the identified peaks.

Quasiperiodicity is different from strict periodicity, such as that identified in Section 5, as they typically manifest as semi-cyclic peaks within a single burst as opposed to strict periodic separation between bursts. Quasiperiodicity is tested with an autocorrelation function where the time lag is calculated with respect to autocorrelation power. Specifically, we employ the `numpy.correlate` (Harris et al. 2020) function on the dedispersed band-averaged time series of each burst. This is defined by

$$c_k = \sum_n a_{n+k} \cdot \bar{a}_n, \tag{A2}$$

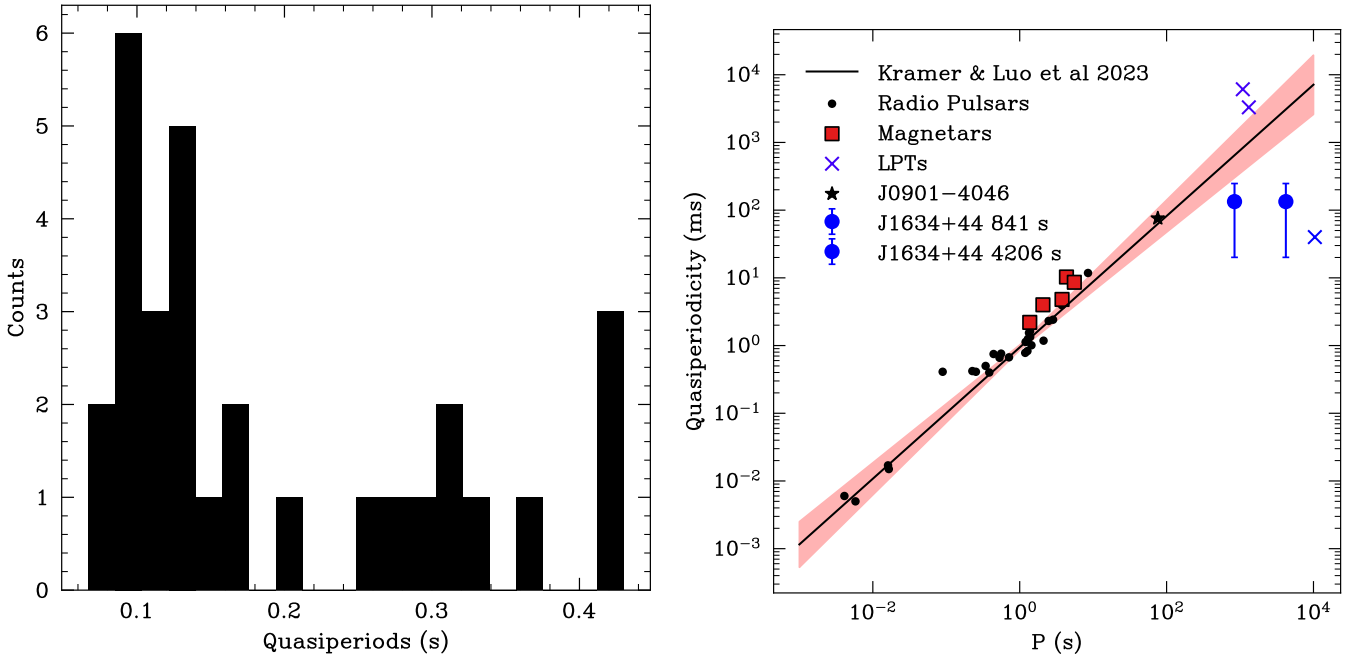

Figure 8. Left panel: A histogram of all the quasiperiods measured for CHIME J1634+44. Right panel: The relationship between quasiperiodicity and period. Due to the log scale, the errors at the rightmost of this figure are large. J1634+44 does not fall within the neutron star quasiperiod region.

where c_k is the correlation function and a is the dedispersed band-averaged time series. $\bar{a}$ denotes complex conjugation, though our intensity time series is strictly real.

In addition to autocorrelation, we also perform a discrete Fast Fourier Transform (FFT) on each time series. This is done via the `sigpyproc`[4] package. Only peaks greater than 3σ are counted towards potential quasiperiodicity. Taking the largest peak identified in the FFT, we mark each timelag where we expect to see a peak in the autocorrelation. This is shown in Figure 7. This was verified manually, as sometimes a higher order harmonic of the actual quasiperiod may be mistakenly identified by the FFT. In all cases, only quasiperiodicities above 3 σ in the FFT are considered. Quasiperiods are collated for all bursts and plotted in Figure 8.

Kramer et al. (2024) showed that almost all variants of isolated neutron stars fit a quasiperiod-period relation; this can include millisecond pulsars, slow pulsars, Rotating Radio Transients (RRATs) and magnetars. Indeed,PSR J0901–4046, an LPT with a spin period of 76 s, and assumed to be a magnetar (Caleb et al. 2024) sits well within the error region of the quasiperiod-period relation. The median quasiperiod for CHIME J1634+44 is $P_\mu = 0.13(0.11)$ s. In Figure 8 we show CHIME J1634+44 amongst other NSs and LPTs with both the ∼4206 s and the ∼841 s period. This shows that CHIME J1634+44 is well outside the error region of the relation, especially if we assume the ∼4206 s period. This may hint that CHIME J1634+44 is unlikely to be an isolated neutron star.

B. PERIOD AMBIGUITY

B.1. *Simulations*

We noticed that when CHIME J1634+44 enters an activity window, it mostly bursts every second day. We define an activity window as when bursts are separated by, at most, 10 days. That is, if there were four bursts on day 1, 8, 13, and 100, there is an activity window from days 1–13 and a new one beginning on day 100. This is robust as bursts come in clusters where the intra-cluster separation is generally much less than 10 days and the inter-cluster separation is generally much larger. As stated above, this repetition fits a beat frequency between 4206 s and CHIME's daily observation cadence. The spin period of 4206 s was also identified by Bloot et al. (2025). However, as shown in

[4] https://github.com/FRBs/sigpyproc3

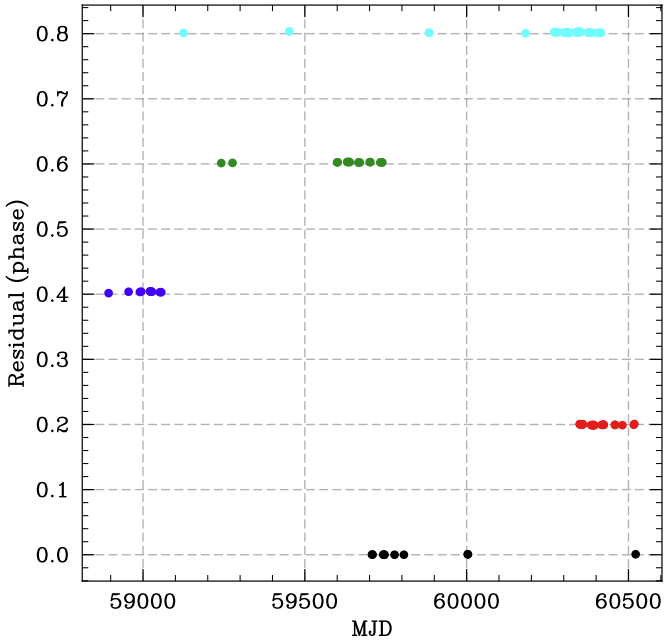

Figure 9. TOA residuals for all the detections made given a 4206 s period, without any phase jumps included. This shows that all bursts are arriving at a multiple of 841 s, that is, bursts arrive at multiples of 0.2 in phase. The colors represent the phase bins to which they belong.

Figure 9, taking all the data into account, it is clear that the bursts are not phase connected with a period of 4206 s. Therefore, we asked the following question: "If CHIME J1634+44 indeed possesses a period of 841 s, how likely is it to see the burst pattern we observe with CHIME?". This question is simplified by the fact that due to CHIME's short transit duration, if CHIME J1634+44 was persistently bursting with a 841 s period, we would detect it once per day, every day. On the contrary, if CHIME J1634+44 were to persistently burst with a 4206 s period, we should detect it every second day. To answer this question, we performed the following steps:

1. For our observed bursts with CHIME, we define an arbitrary activity period of 10 days. That is, if bursts are detected within 10 days, we consider the bursts part of the same activity period.
2. We form consecutive pairs of bursts and count how many such pairs are detected to agree with *only* the 841 s period (i.e., the pairs are separated by an odd number of days). We ignore all burst pairs that are not part of the same activity period.
3. We find that there are 60 burst pairs, 11 of which agree *only* with the 841 s period, and 49 of which agree with both the 841 s and 4206 s period.
4. We assume that if the period is truly 841 s then we would expect to find the separation between bursts to be equally as likely to be an odd number of days or an even number of days. That is, at each 841 s epoch, there is a 50% chance a burst will occur.
5. We simulate 1,000,000 iterations of 60 burst pairs and count the number of even and odd-day burst separations.
6. We find that the mean number of odd-day burst separations is 33.35 with a standard deviation of 3.86. Therefore, our observations are $\sim$ 5.8 standard deviations away from the mean, with a probability of 3.5×10^{-9}. This is shown in Figure 10.

To summarize, our simulations show that it is highly unlikely for CHIME J1634+44 to be an isolated "normal" 841 s LPT and create the burst patterns that are observed. We conclude that additional, unknown physical mechanisms, such as orbital resonances, must be invoked to explain our observations. We note that Bloot et al. (2025) proposed a possible 5:2 spin-orbit resonance with an orbital period of $\sim$2103.1 s. We find no evidence of this orbital period in our timing data.

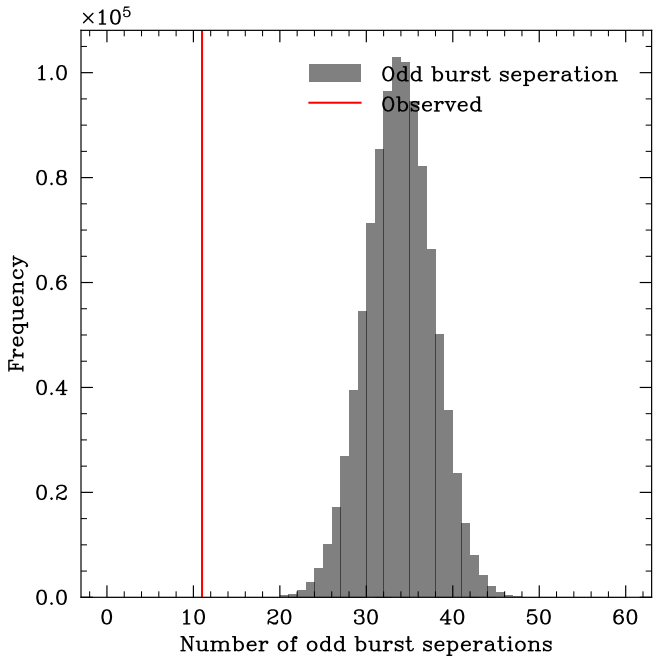

Figure 10. The distribution of the number of odd-day burst separations for 1,000,000 simulations of 60 burst pairs. The red line shows the observed number of odd burst separations.

C. SWIFT X-RAY AND UV

Upon the detection of an activity period beginning in MJD 60270 (2023 November 22), we triggered 10 ks of *Swift* ToO time to observe CHIME J1634+44 on 2023 December 07 and 2024 January 04 (target ID 16412). The data (XRT/Photon Counting mode) were processed with the `UK Swift Science Data Centre`[5] online tool (Evans et al. 2020). In total, 6 sources were detected across the 0.3-10 keV band in the field of view of Swift/XRT; however, none were within a 3-σ error region of CHIME J1634+44. We then used the upper limit server[6], which utilizes the corresponding data (for a set of input coordinates), the background map, and the exposure map to determine an upper limit on the 0.2–10.0 keV count rate of 1.8×10^{-3} c/s (Evans et al. 2020). In order to derive physically meaningful comparisons, we utilized the `WebPIMMS` tool to calculate the flux upper limit for CHIME J1634+44. We assumed $N_H = 7.5 \times 10^{20}$ cm^{-2} (based on the source DM and the N_H-DM relation; He et al. 2013), and either a blackbody spectrum with $kT = 0.3$ keV or a power law spectrum with $\Gamma = 1$. These values are representative of a magnetar (Hurley-Walker et al. 2022) or an intermediate polar (WD with MS companion; Rodriguez et al. 2023). We found that with a 3-σ upper limit on the 0.2–10.0 keV count rate of 1.8×10^{-3} c/s, the corresponding 0.3–10 keV unabsorbed flux upper limit is 4.8×10^{-14} ergs cm^{-2} s^{-1} for a $kT = 0.3$ keV blackbody and 1.2×10^{-13} ergs cm^{-2} s^{-1} for a power law with $\Gamma = 1$. This is then converted to an upper limit on the 0.2–10 keV luminosity of 5.2×10^{31} ergs s^{-1} or 1.3×10^{32} ergs s^{-1}, respectively. We discuss the implications for the X-ray counterpart in Section 6.2.

Concurrently, *Swift* provided Ultra-violet Optical Telescope (UVOT) data with the UVM2 filter centered on 2246Å. Unfortunately, only 1508 s of the 10 ks were available. No detections were made in the VLA localization region. We derive a 5-σ upper limit of $m_{AB} > 21.69$.

[5] https://www.swift.ac.uk/user_objects/

[6] https://www.swift.ac.uk/LSXPS/ulserv.php

REFERENCES

Aihara, H., AlSayyad, Y., Ando, M., et al. 2022, PASJ, 74, 247, doi: 10.1093/pasj/psab122

Andersen, B. C., Patel, C., Brar, C., et al. 2023, AJ, 166, 138, doi: 10.3847/1538-3881/acec78

Barrett, P., Dieck, C., Beasley, A. J., Mason, P. A., & Singh, K. P. 2020, Advances in Space Research, 66, 1226, doi: 10.1016/j.asr.2020.04.007

Beniamini, P., Wadiasingh, Z., Hare, J., et al. 2023, MNRAS, 520, 1872, doi: 10.1093/mnras/stad208

Bochenek, C. D., Ravi, V., Belov, K. V., et al. 2020, Nature, 587, 59, doi: 10.1038/s41586-020-2872-x

Brentjens, M. A., & de Bruyn, A. G. 2005, A&A, 441, 1217, doi: 10.1051/0004-6361:20052990

Buckley, D. A. H., Meintjes, P. J., Potter, S. B., Marsh, T. R., & Gänsicke, B. T. 2017, Nature Astronomy, 1, 0029, doi: 10.1038/s41550-016-0029

Burdge, K. B., Coughlin, M. W., Fuller, J., et al. 2019a, Nature, 571, 528, doi: 10.1038/s41586-019-1403-0

Burdge, K. B., Fuller, J., Phinney, E. S., et al. 2019b, ApJL, 886, L12, doi: 10.3847/2041-8213/ab53e5

Burn, B. J. 1966, MNRAS, 133, 67, doi: 10.1093/mnras/133.1.67

Caleb, M., Heywood, I., Rajwade, K., et al. 2022, Nature Astronomy, 6, 828, doi: 10.1038/s41550-022-01688-x

Caleb, M., Lenc, E., Kaplan, D. L., et al. 2024, Nature Astronomy, 8, 1159, doi: 10.1038/s41550-024-02277-w

CHIME Collaboration, Amiri, M., Bandura, K., et al. 2022, ApJS, 261, 29, doi: 10.3847/1538-4365/ac6fd9

CHIME/FRB Collaboration, Amiri, M., Bandura, K., et al. 2018, ApJ, 863, 48, doi: 10.3847/1538-4357/aad188

CHIME/FRB Collaboration, Andersen, B. C., Bandura, K. M., et al. 2020, Nature, 587, 54, doi: 10.1038/s41586-020-2863-y

CHIME/FRB Collaboration, Amiri, M., Andersen, B. C., et al. 2024a, ApJ, 969, 145, doi: 10.3847/1538-4357/ad464b

—. 2024b, ApJ, 969, 145, doi: 10.3847/1538-4357/ad464b

CHIME/Pulsar Collaboration, Amiri, M., Bandura, K. M., et al. 2021, ApJS, 255, 5, doi: 10.3847/1538-4365/abfdcb

Cognard, I., Shrauner, J. A., Taylor, J. H., & Thorsett, S. E. 1996, ApJL, 457, L81, doi: 10.1086/309894

Cordes, J. M., & Lazio, T. J. W. 2002, arXiv e-prints, astro, doi: 10.48550/arXiv.astro-ph/0207156

Coti Zelati, F., Rea, N., Pons, J. A., Campana, S., & Esposito, P. 2018, MNRAS, 474, 961, doi: 10.1093/mnras/stx2679

Cusumano, G., Hermsen, W., Kramer, M., et al. 2003, A&A, 410, L9, doi: 10.1051/0004-6361:20031368

de Ruiter, I., Rajwade, K. M., Bassa, C. G., et al. 2025, Nature Astronomy, doi: 10.1038/s41550-025-02491-0

Dong, F. 2024, PhD thesis, University of British Columbia, doi: http://dx.doi.org/10.14288/1.0445624

Dong, F. A., Clarke, T., Curtin, A. P., et al. 2024, arXiv e-prints, arXiv:2407.07480, doi: 10.48550/arXiv.2407.07480

Dulk, G. A. 1985, ARA&A, 23, 169, doi: 10.1146/annurev.aa.23.090185.001125

Enoto, T., Terasawa, T., Kisaka, S., et al. 2021, Science, 372, 187, doi: 10.1126/science.abd4659

Evans, P. A., Page, K. L., Osborne, J. P., et al. 2020, ApJS, 247, 54, doi: 10.3847/1538-4365/ab7db9

Falanga, M., Kuiper, L., Poutanen, J., et al. 2005, A&A, 444, 15, doi: 10.1051/0004-6361:20053472

Hallinan, G., Antonova, A., Doyle, J. G., et al. 2008, ApJ, 684, 644, doi: 10.1086/590360

Hallinan, G., Bourke, S., Lane, C., et al. 2007, ApJL, 663, L25, doi: 10.1086/519790

Han, J. L., Manchester, R. N., Xu, R. X., & Qiao, G. J. 1998, MNRAS, 300, 373, doi: 10.1046/j.1365-8711.1998.01869.x

Harris, C. R., Millman, K. J., van der Walt, S. J., et al. 2020, Nature, 585, 357, doi: 10.1038/s41586-020-2649-2

Haslam, C. G. T., Salter, C. J., Stoffel, H., & Wilson, W. E. 1982, A&AS, 47, 1

He, C., Ng, C. Y., & Kaspi, V. M. 2013, ApJ, 768, 64, doi: 10.1088/0004-637X/768/1/64

Helfand, D. J., White, R. L., & Becker, R. H. 2015, ApJ, 801, 26, doi: 10.1088/0004-637X/801/1/26

Hu, C.-P., Ng, C. Y., & Ho, W. C. G. 2019, MNRAS, 485, 4274, doi: 10.1093/mnras/stz513

Hurley-Walker, N., Zhang, X., Bahramian, A., et al. 2022, Nature, 601, 526, doi: 10.1038/s41586-021-04272-x

Hurley-Walker, N., Rea, N., McSweeney, S. J., et al. 2023, Nature, 619, 487, doi: 10.1038/s41586-023-06202-5

Hurley-Walker, N., McSweeney, S. J., Bahramian, A., et al. 2024, ApJL, 976, L21, doi: 10.3847/2041-8213/ad890e

Hutschenreuter, S., Anderson, C. S., Betti, S., et al. 2022, A&A, 657, A43, doi: 10.1051/0004-6361/202140486

Jaodand, A., Hessels, J. W. T., & Archibald, A. 2018, in IAU Symposium, Vol. 337, Pulsar Astrophysics the Next Fifty Years, ed. P. Weltevrede, B. B. P. Perera, L. L. Preston, & S. Sanidas, 47–51, doi: 10.1017/S1743921317010407

Jiang, J. C., Xu, J. W., Niu, J. R., et al. 2024, National Science Review, 12, nwae293, doi: 10.1093/nsr/nwae293

Johnston, S., Romani, R. W., Marshall, F. E., & Zhang, W. 2004, MNRAS, 355, 31, doi: 10.1111/j.1365-2966.2004.08286.x

Katz, J. I. 2022, Ap&SS, 367, 108, doi: 10.1007/s10509-022-04146-2

Kramer, M., Liu, K., Desvignes, G., Karuppusamy, R., & Stappers, B. W. 2024, Nature Astronomy, 8, 230, doi: 10.1038/s41550-023-02125-3

Law, C. J., Bower, G. C., Burke-Spolaor, S., et al. 2018, ApJS, 236, 8, doi: 10.3847/1538-4365/aab77b

Lee, Y. W. J., Caleb, M., Murphy, T., et al. 2025, Nature Astronomy, 9, 393, doi: 10.1038/s41550-024-02452-z

Li, D., Yuan, M., Wu, L., et al. 2024, arXiv e-prints, arXiv:2411.15739, doi: 10.48550/arXiv.2411.15739

Lo, K. K., Bray, J. D., Hobbs, G., et al. 2012, MNRAS, 421, 3316, doi: 10.1111/j.1365-2966.2012.20555.x

Lorimer, D. R., & Kramer, M. 2012, Handbook of Pulsar Astronomy

Luo, J., Ransom, S., Demorest, P., et al. 2021, ApJ, 911, 45, doi: 10.3847/1538-4357/abe62f

Maan, Y., Joshi, B. C., Surnis, M. P., Bagchi, M., & Manoharan, P. K. 2019, ApJL, 882, L9, doi: 10.3847/2041-8213/ab3a47

Manchester, R. N., & Lyne, A. G. 1977, MNRAS, 181, 761, doi: 10.1093/mnras/181.4.761

Manchester, R. N., & Taylor, J. H. 1977, Pulsars

Marques, M. S., Zarka, P., Echer, E., et al. 2017, A&A, 604, A17, doi: 10.1051/0004-6361/201630025

Marsh, T. R., Gänsicke, B. T., Hümmerich, S., et al. 2016, Nature, 537, 374, doi: 10.1038/nature18620

Martin, D. C., Fanson, J., Schiminovich, D., et al. 2005, ApJL, 619, L1, doi: 10.1086/426387

Mckinven, R., Michilli, D., Masui, K., et al. 2021, ApJ, 920, 138, doi: 10.3847/1538-4357/ac126a

Mckinven, R., Bhardwaj, M., Eftekhari, T., et al. 2024, arXiv e-prints, arXiv:2402.09304, doi: 10.48550/arXiv.2402.09304

Michilli, D., Masui, K. W., Mckinven, R., et al. 2021, ApJ, 910, 147, doi: 10.3847/1538-4357/abe626

Nimmo, K., Pleunis, Z., Beniamini, P., et al. 2025, Nature, 637, 48, doi: 10.1038/s41586-024-08297-w

Olausen, S. A., Zhu, W. W., Vogel, J. K., et al. 2013, ApJ, 764, 1, doi: 10.1088/0004-637X/764/1/1

Paice, J. A., Scaringi, S., Castro Segura, N., et al. 2024, MNRAS, 531, L82, doi: 10.1093/mnrasl/slae035

Pandhi, A., Pleunis, Z., Mckinven, R., et al. 2024, ApJ, 968, 50, doi: 10.3847/1538-4357/ad40aa

Papitto, A., & de Martino, D. 2022, in Astrophysics and Space Science Library, Vol. 465, Astrophysics and Space Science Library, ed. S. Bhattacharyya, A. Papitto, & D. Bhattacharya, 157–200, doi: 10.1007/978-3-030-85198-9_6

Pelisoli, I., Marsh, T. R., Buckley, D. A. H., et al. 2023, Nature Astronomy, 7, 931, doi: 10.1038/s41550-023-01995-x

Pineda, J. S., & Villadsen, J. 2023, Nature Astronomy, 7, 569, doi: 10.1038/s41550-023-01914-0

Purcell, C. R., Van Eck, C. L., West, J., Sun, X. H., & Gaensler, B. M. 2020, RM-Tools: Rotation measure (RM) synthesis and Stokes QU-fitting, Astrophysics Source Code Library, record ascl:2005.003

Qu, Y., & Zhang, B. 2023, MNRAS, 522, 2448, doi: 10.1093/mnras/stad1072

Rea, N., Hurley-Walker, N., Pardo-Araujo, C., et al. 2024, ApJ, 961, 214, doi: 10.3847/1538-4357/ad165d

Rodriguez, A. C. 2025, A&A, 695, L8, doi: 10.1051/0004-6361/202553684

Rodriguez, A. C., Galiullin, I., Gilfanov, M., et al. 2023, ApJ, 954, 63, doi: 10.3847/1538-4357/ace698

Rucinski, S. M. 1994, AcA, 44, 75

Salcedo, C., Mori, K., Bridges, G., et al. 2024, ApJ, 976, 115, doi: 10.3847/1538-4357/ad7feb

Schaefer, B. E. 2024, ApJ, 966, 155, doi: 10.3847/1538-4357/ad31a9

Schreiber, M. R., Belloni, D., Gänsicke, B. T., Parsons, S. G., & Zorotovic, M. 2021, Nature Astronomy, 5, 648, doi: 10.1038/s41550-021-01346-8

Shimwell, T. W., Tasse, C., Hardcastle, M. J., et al. 2019, A&A, 622, A1, doi: 10.1051/0004-6361/201833559

Shimwell, T. W., Hardcastle, M. J., Tasse, C., et al. 2022, A&A, 659, A1, doi: 10.1051/0004-6361/202142484

Solheim, J. E. 2010, PASP, 122, 1133, doi: 10.1086/656680

Tanaka, M., Ikeda, H., Murata, K., et al. 2021, PASJ, 73, 735, doi: 10.1093/pasj/psab034

Vedantham, H. K., & Ravi, V. 2019, MNRAS, 485, L78, doi: 10.1093/mnrasl/slz038

Wang, Z., Rea, N., Bao, T., et al. 2024, arXiv e-prints, arXiv:2411.16606, doi: 10.48550/arXiv.2411.16606

Warner, B. 1995, Cataclysmic variable stars, Vol. 28

White, R. L., Becker, R. H., Helfand, D. J., & Gregg, M. D. 1997, ApJ, 475, 479, doi: 10.1086/303564

Wijnands, R., & van der Klis, M. 1998, Nature, 394, 344, doi: 10.1038/28557

Yao, J. M., Manchester, R. N., & Wang, N. 2017, ApJ, 835, 29, doi: 10.3847/1538-4357/835/1/29